Characterization of Oxides of Cesium

A. Band,[†] A. Albu-Yaron,[†] T. Livneh,[†,‡] H. Cohen,[§] Y. Feldman,[§] L. Shimon,[§] R. Popovitz-Biro,[†] V. Lyahovitskaya,[†] and R. Tenne*[,†]

Department of Materials and Interfaces and Chemical Services Unit, Weizmann Institute of Science, Rehovot 76100, Israel

Received: August 14, 2003; In Final Form: March 10, 2004

Cesium oxides are materials of great interest to the photodetection industry because of their relatively low work function (∼1 eV). Used mainly as coating films for photoemissive devices, they provide high wavelength thresholds and high photocurrents. However, they are unstable, air-sensitive, and hygroscopic, rendering them short-lived and limiting their applications. Although the technology of these devices is highly developed, their characterization on the micro- and nanoscale suffers from their poor chemical stability and poor crystallinity. In the present study, cesium oxides were synthesized from the elements and were characterized using a combination of chemical and structural analysis techniques. Because the reaction products were extremely sensitive to humidity, sample analysis without atmospheric exposure was essential, and techniques were developed for the transfer of the samples to the measurements systems. Extensive data obtained from X-ray energy-dispersive spectroscopy (EDS), X-ray photoelectron spectroscopy (XPS), transmission electron microscopy (TEM), selected-area electron diffraction (SAED), X-ray diffraction (XRD), and Raman microscopy were obtained. Raman spectra with bands at 103, 742, and 1134 cm^{-1} strongly confirmed the presence of the oxide, peroxide, and superoxide ions, respectively, as well as the absence of carbonate as an impurity. The A_{1g} mode of Cs_2O was detected as an anti-Stokes band at 103 cm^{-1}. This study provides further insight into the reactivity of the various cesium oxides.

Introduction

The oxidation of alkali metals is a field of great technological interest as alkali metal−oxygen compounds play a crucial role in the engineering of photocathodes, in the promotion of catalytic reactions, and in the oxidation enhancement of semiconductor surfaces. In particular, the oxides of cesium play an important role in many practical photoemissive devices. The oxides of cesium are low-work-function semiconductors. The low work function enables the electrons to escape from the solid upon low-energy excitations and create photoemissive surfaces suitable for light detection with high quantum efficiency and high threshold wavelengths.

The complex cesium−oxygen phase diagram consists of an unusually large number of oxides: the suboxides (e.g., Cs_7O, Cs_4O, Cs_3O, and Cs_7O_2), the normal oxide (Cs_2O), the sesquioxide (Cs_2O_3), and the per- and superoxides (Cs_2O_2, CsO_3, and Cs_2O_4 or CsO_2). Furthermore, no clear relationship has been found between the Cs/O ratios and the measured work functions.

Various studies during the early 1900s described procedures for the synthesis of pure cesium oxides.[1−4] Later studies revealed the crystal structures of these oxides.[5−9] More recent investigations of these materials applying ultraviolet and X-ray photoelectron spectroscopies (UPS and XPS, respectively) and nuclear magnetic resonance (NMR) techniques suggest that the earlier characterizations of the various cesium oxide compounds were, in fact, oversimplified.[10−14] Cesium oxides are highly unstable in air. In particular, the reaction of cesium and its oxides with residual CO_2 gas and humidity is highly exothermic. Therefore, these materials must be studied under a strictly inert or vacuum environment. This limitation and the complexity of the phase diagram makes the comprehensive characterization of these materials rather important but a very difficult task.

The cesium oxides' band-gap energies (E_g) and electron affinities (EA) are not accurately known. From light absorption and photoemission measurements, Borzyak et al. made reasonable estimates for Cs_2O: $E_g = 2$ eV and EA = 0.8 eV.[15] Sommer measured work functions as low as 1 eV (∼1200 nm) for mixtures of cesium oxides.[10] Many studies have been performed to improve the properties of cesium oxide films as coatings for photocathode front surfaces. Aging of the photocathodes is often related to degradation of the cesium oxide coating. It was found that the highest photoemissivity and greatest stability of photocathodes is obtained with a cesium-to-oxygen ratio very close to 2:1.[16] However, this ratio does not necessarily indicate the exclusive presence of Cs_2O. The engineering of devices such as photocathodes is focused mostly on achieving the lowest work function and the highest quantum efficiency and not necessarily on optimizing the structure and chemical composition of the deposited films. Furthermore, cesium oxide films are prepared under moderate conditions, and therefore, their crystallinity is quite poor, and their phase not necessarily well-defined, which makes these films yet more sensitive to the atmosphere or to heating.

In the present study, an extensive effort at the characterization of cesium oxides, which was not available before, is presented. The compounds were synthesized directly from the elements.[5] Techniques for manipulating and transferring samples from the reaction vessel to the analysis apparatus under strictly inert

* To whom correspondence should be addressed. E-mail: reshef.tenne@weizmann.ac.il.

[†] Department of Materials and Interfaces.

[‡] Permanent address: Nuclear Research Center-Negev, Beer Sheva, P.O. Box 9001, Beer Sheva, Israel 84190.

[§] Chemical Services Unit.

10.1021/jp036432o CCC: $27.50
Published on Web 07/27/2004

conditions of an anhydrous/anaerobic atmosphere were developed, enabling their characterization by transmission electron microscopy, which had not been reported previously for these materials. Chemical analyses of the products were carried out by X-ray energy-dispersive spectroscopy (EDS) and X-ray photoelectron spectroscopy (XPS) measurements. Structural analysis was achieved by X-ray diffraction (XRD) and electron diffraction (ED), as well as by transmission electron microscopy (TEM). Raman microscopy and absorption and luminescence measurements were carried out to gain additional information on the products. This unique combination of divergent analytical techniques and the extensive data obtained allowed for a firm identification of the major reaction products and sources of contamination, such as carbonates, that occurred during the synthesis and handling of the samples.

Experimental Section

Materials. Cesium metal (>98%) was purchased from Metals Basis, Alfa Aesar, and oxygen gas (>98%) from Hamercaz Lehamzan Ltd., Herzliya, Israel.

Synthesis. All syntheses in this work were carried out in quartz or Pyrex ampules. Cesium was transferred to the ampule, which was terminated with a high-pressure Teflon valve (Rotaflo, Stoke-on-Trent, Staffordshire, U.K.), under argon atmosphere in a dry glovebox. The ampules were first evacuated to 10^{-5} Torr, and a measured (corresponding to Cs_2O stoichiometry) amount of oxygen gas was added. After the addition of oxygen, the ampules were sealed, and their contents were heated to 250 °C overnight. Cooling to room temperature was done at a controlled rate of 0.1 °C/min. In the attempt to reach mainly a cesium/oxygen ratio of 2:1 of the final synthesized product, modifications of the above basic procedure were tried by varying the oxygen content, the reaction temperature (100−600 °C), and/or the final cooling rate or in a few cases by quenching in liquid nitrogen. Over 70 synthesis experiments were carried out under these various experimental conditions. An initial visual inspection overview of the resulting solid powders of all of the performed syntheses indicates inhomogeneities in their respective colors (between and within the ampules). The chemical and structural analysis reported here, however, refers to the materials resulting from the same synthesis procedure, described above, but each performed on different batches (ampules). The direct cesium oxidation products issued from the synthesis procedure used in this work exhibited mainly dark purple and to a lesser extent orange colors.

Analysis. *Optical Absorption and Luminescence.* Measurements were carried out on sealed ampules with flat surfaces. A double-grating monochromator (HRD, Jobin-Yvon) with a standard tungsten lamp was used along with a photomultiplier (RG942, Hamamatsu). Both absorption and luminescence (excitation with an Ar ion laser at 514.5 nm) were measured in the range of 500−900 nm at room temperature.

Raman Microscopy. Measurements were carried out directly on the sealed reaction ampules. Raman measurements were performed with a Raman imaging microscope (Renishaw 1000) equipped with a 25-mW He−Ne 632.8-nm laser.

X-ray diffraction was performed on samples transferred to thin-wall quartz capillaries. An Enraf Nonius FR590 generator with sealed-tube molybdenum radiation ($\lambda = 0.71$ Å) was used for powder X-ray diffraction. The generator was set to a voltage of 50 kV and a current of 30 mA.

Transmission Electron Microscopy (TEM). Imaging, electron diffraction (ED), and chemical analysis by X-ray energy-dispersive spectroscopy (EDS) of the products were performed with a Phillips CM120 TEM (tungsten filament) instrument operated at 120 kV, fitted with an EDAX system (model Phoenix) and application programs. The samples were transferred from the reaction ampule to a desiccator in the glovebox. The desiccator was subsequently loaded into an inflatable glovebag filled with argon for mounting of the specimens onto copper grids coated with either carbon or lacey carbon films. A sleeve connected the glovebag to the goniometer of the microscope, permitting transfer of the grids to the TEM instrument without exposing them to the room atmosphere.

X-ray Photoelectron Spectroscopy (XPS). Measurements were performed in an AXIS-HS Kratos Analytical instrument, using a monochromatized Al (Kα) source, $h\nu = 1486.6$ eV. The line shapes were analyzed by curve fitting of the experimental data using Gaussian−Lorentzian functions and Shirley background subtraction. A special sample holder was manufactured to transfer the air-sensitive samples from the argon glovebox into the XPS chamber under medium (10^{-2} Torr) vacuum conditions. A rough estimate of the transfer quality could be obtained visually from the color of the powder within the analysis chamber. Of the four samples analyzed by XPS, two samples underwent a successful transfer. The analysis of the best sample, number 10, is presented below. Light Ar sputtering was still needed (4 keV, rate of ∼50 Å/min) to remove adsorbed carbon and oxygen from the surface, enabling a distinction between surface and bulk compositions.

Notwithstanding the lengthy synthetic process, the chemical composition of the samples was not uniform and was found to vary from one location to another within the ampule. The wide array of analytical methods engaged in this work, however, was undertaken to achieve the characterization of these inhomogeneous and reactive oxide phases. Each analytical technique probed a different typical sample area (volume): EDS on TEM and micro-Raman and XPS measurements probe areas of approximately 100 nm^2, 10 μm^2, and 1 mm^2, respectively. XRD measurements were performed on areas of a few square millimeters. Therefore, the EDS and to some extent also the micro-Raman techniques were used to characterize single phases. The differences in depth sensitivity of the above techniques were used as a complementary source of information regarding the depth distribution of the various products. For example, EDS was not sensitive to the superficial cesium carbonate film that was found by the XPS and TEM/ED analyses. This film could have been obtained during the transfer of the sample to the XPS, or it might have always been present on the sample surface.

Results

Over 70 synthesis experiments were carried out under various conditions. To rationalize the experimental findings, the results presented in this study are restricted only to the synthesis performed at a Cs/O ratio of 2:1, at a heating temperature of 250 °C, and at a cooling rate of 0.1 °C/min. The inhomogeneity of the resulting solid powders was manifested by their different colors. For example, the products of samples 1, 2, 5−8, 12, 13, and 60 were dark purple, whereas those of samples 3, 4, 9−11, 14, 15, 22, and 39 were partially orange, with most of the material nevertheless being purple. Furthermore, the colors of samples that were exposed to ambient atmosphere changed to white instantaneously, and their composition matched that of cesium carbonate. Comprehensive examination of the products by chemical and structural analysis techniques leading to the identification of a mixture of several oxides is hereby presented. Note that, because of the very high reactivity of the material

TABLE 1: Cs/O Ratios in Different Synthesized Materials Calculated from EDS Spectra

sample	cesium (%)	oxygen (%)	Cs/O	oxide formula[a]
1	39.2	60.8	1.0:1.5	Cs_2O_3
2	42.0	58.0	1.0:1.4	
3	36.8	63.2	1.0:1.7	
4 (position a)	46.5	53.5	1.0:1.1	Cs_2O_2
4 (position b)	23.2	76.8	1.0:3.3	CsO_3
5	22.8	77.2	1.0:3.4	
6	24.0	76.0	1.0:3.2	
7	32.3	67.7	1.0:2.1	CsO_2
8	32.9	67.1	1.0:2.0	
9	62.9	37.1	1.7:1.0	Cs_2O

[a] Suggested oxide according to the O/Cs stoichiometric ratio.

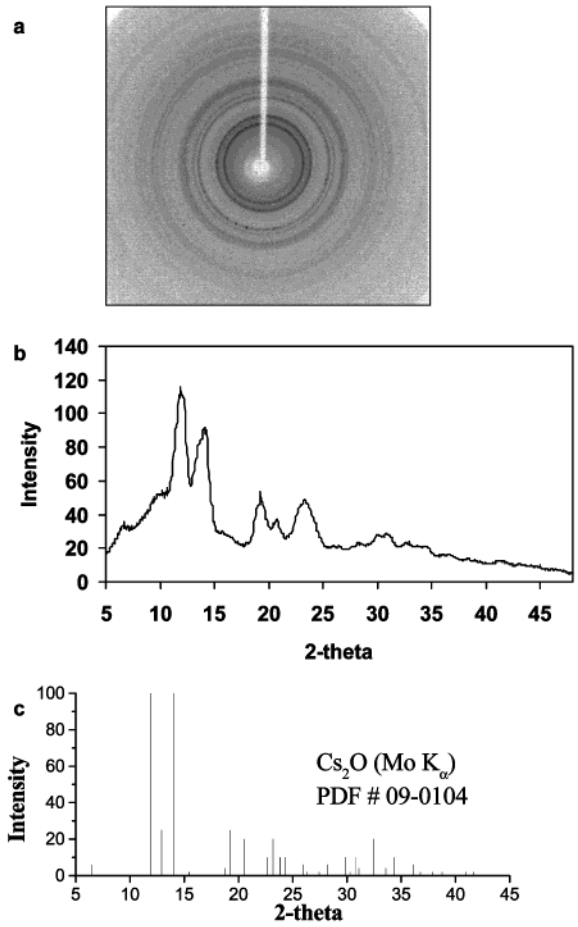

Figure 1. XRD pattern of cesium oxide powder from sample 11. (a) Raw data, (b) intensity profile, (c) peak positions according to PDF #09-0104.

and the location (sometime 500 m apart) of the different instruments used, it was not possible to perform more than one analysis on a single opened ampule (sample).

Chemical Characterization. Results obtained by EDS analyses of various structural features observed in some of the synthesized materials are summarized in Table 1: apparent relative concentrations are listed as Cs/O ratios and represent the average of three to five measurements. EDS analysis on typical areas of ~100 nm^2 revealed that the examined samples had more than one type of oxide present, as reflected also in the XRD and ED analyses (Figure 1 and Table 2). The variations in the Cs/O ratio at different locations of a sample and from sample to sample reflect the inhomogeneity of the synthesized materials. Also, in most cases, the oxygen content was higher than expected according to the assigned oxides. This discrepancy is ascribed to the presence of adsorbed oxygen on the TEM grid itself and/or on the sample surface (possibly hydrates).

Chemical analysis by XPS provided further evidence of the inhomogeneity of the samples. The analyzed powder (sample 10) was mostly orange-tinted, but the ampule contained substantial amounts of the deep purple phase, which could have been mixed with the orange powder during processing of the ampule contents and transfer to the XPS instrument. The presence of Cs_2O, in addition to Cs_2O_2 and CsO_2, was confirmed by these measurements. No significant material degradation was detected during the XPS measurements. Although the samples were measured under ultrahigh vacuum (10^{-8}–10^{-9} Torr), the outer layer of the material reacted to give cesium carbonate and cesium carbide, which were removed by a very short low dose Ar ion sputtering.

Table 3 presents the results of XPS measurements carried out on one of the synthesized materials (sample 10). The C 1s and the O 1s spectra of carbon and oxygen consist of broad lines that could be decomposed into several components. The carbon peak at ~282 eV is assigned to cesium carbide,[17] whereas the carbon adsorbed on the surface of the material appears at a binding energy of 284.8 eV and was used to calibrate the energy scale. This signal is dramatically decreased after sputtering. The carbon peak at approximately 288 eV is attributed to CO_3^{2-} groups.[18,19] The oxygen peaks are assigned to the negative oxygen ions according to Jupille et al.,[13] who studied thick oxidized Cs layers by XPS. The present results are in very good agreement with previously published data. The presence of these ions clearly supports the claim that microcrystalline particles of cesium oxide, cesium peroxide, and cesium superoxide are constituents of the reaction products. From the assignment of the different peaks, it is possible to conclude that, in the area of the measurements, CsO_2 is the most abundant product as the superoxide ion is detected with the highest percentage. Yet, Ar sputtering shows that the sample surface is typically more oxidized than the bulk material. The outermost surface consists of CsO_2, whereas the depth profile tends to lead to 1:1 stoichiometry of Cs/O. This ratio is sometimes spoiled by reoxidation of the sputtered surface by residual oxygen in the vacuum chamber. Cs_2O and Cs_2O_2 are identified by the O^{2-} and O_2^{2-} binding energies (525.3 and 530.5 eV), respectively. The distribution between the oxides can be estimated from the ratio between the oxygen ions peaks: $Cs_2O/Cs_2O_2/CsO_2 = 1.1:1.0:5.0$. Because of the large analyzed area (1 mm^2), microscopic crystals could not be examined separately. As expected, less successful transfers of the sample exhibited enhanced surface oxidation, i.e., enrichment with respect to CsO_2, and the presence of carbonates.

An interesting in situ result emerged from XPS measurements obtained under illumination. The light-induced XPS (LIXPS) analysis[20] provides information on photoconductivity and hence on the optical properties of the sample. Using a HeNe laser source (1.96 eV), the studied powder exhibited significant light-induced line shifts, which indicate efficient optical absorption of red light. These complementary in situ data confirm the relevance of the XPS analysis to the optical study of the sealed material (see Figure 6 below).

Structural Characterization. *XRD and TEM.* The X-ray diffraction pattern of an orange sample (11) held in a quartz capillary, obtained with an Enraf Nonius diffractometer, is presented in Figure 1a. The peaks in the pattern (Figure 1b) can be indexed according to (*hkl*) lines of Cs_2O (PDF #09-0104) (Figure 1c). The widths of the peaks reflect the small size of the Cs_2O nanoparticles. The XRD patterns of the two other

TABLE 2: Experimental *d* Spacings (Å) Calculated from Electron Diffraction Data of the Two Sets of Ring Patterns Compared with *d* Spacings of the Corresponding PDFs of the Cesium Oxide Phases

calculated *d* spacings set 1		*d* spacings from PDFs						calculated *d* spacings set 2	
sample		cesium oxide phase						sample	
12	13	CsO_3	CsO_2	Cs_2O_3	Cs_2O_2	Cs_2O	Cs_2CO_3	14	15
							5.14	5.16	5.12
							4.23	4.29	4.23
3.77			3.81[a]						
					(−[b]) 3.57[a]				
				3.49[a]		3.43[a]	3.45	3.46	3.50
3.19			3.16[a]	3.12[a]		3.16	3.15	3.13	3.14
		(−[b]) 3.10[a]							
							3.05[a]	3.05	
							(−[b]) 2.99[a]		
						2.91[a]		2.89	2.89
2.78		2.79[a]							
	2.70								
				2.63[a]	2.58[a]		2.61[a]	2.57	2.58
		(−[b]) 2.42[a]		2.47	2.43[a]		2.45	2.46	2.47
2.34		2.34	2.38[a]						2.39
	2.27		2.23						
				2.10	2.15	2.12	2.17	2.17	2.16
1.99		1.97				2.00		1.98	
			1.93	1.93[a]	1.92		1.95		1.92
					1.78	1.76		1.73	
1.66	1.63	1.62[a]		1.60	1.62[a]	1.58	1.65	1.61	
1.42	1.38	1 1.41	1.41	1.45	1.48	1.45		1.46	
1.35	1.32	1.33	1.32						
1.19	1.16	1.20[a]							
1.06	1.03								
0.97	0.95	0.94							

[a] Asterisks (*) denote peaks of highest intensity in the corresponding PDFs. [b] Dashes (−) denote high-intensity peaks not observed in the electron diffraction patterns.

TABLE 3: XPS Data for Sample 10

		atomic concentration (%)			
element	BE (eV)	fresh sample	30-s sputtered	1-min sputtered	compound
Cs 3d	723.5 ± 0.2	26.8	43.2	46.0	
O 1s	525.3 ± 0.1	1.9	4.7	5.4	O^{2-}
	529.5 ± 0.2	25.6	25.9	24.1	O_2^-
	530.5 ± 0.1	0	2.5	4.8	O_2^{2-}
C 1s	282.7 ± 0.2	10.2	8.4	9.0	CsC
	284.8 ± 0.1	26.8	9.1	5.8	C
	288.1 ± 0.1	8.7	6.2	4.9	Cs_2CO_3

samples studied by this method coincided clearly with CsO_2 as the major phase, along with Cs_2O_2.

Typical selected-area electron diffraction (SAED) patterns obtained by TEM with samples 1−9 and 12−15 are shown in Figure 2. A background of fairly sharp and continuous rings can be discerned in all of the diffraction patterns examined, indicative of the polycrystalline nature of the product. It is noticed that these diffraction rings belong to two sets of diffraction patterns (see Figure 2a,b). Table 2 shows the calculated *d* spacings of the two sets of patterns, together with the corresponding values taken from the powder diffraction files (PDFs) of the various cesium oxide and cesium carbonate phases in samples 12−15. Note that peaks of high intensity in the PDF files are denoted by asterisks (*); high-intensity peaks that do not appear in the ED pattern are denoted by dashes (−). It is clearly observed that there is relatively little overlap between the *d* lines of the two series and that there exist in fact two separate sets of diffraction patterns. "Set 1" (Figure 2a and Table 2) appears to correspond to the characteristic CsO_2 diffraction lines (PDF #26-0395). The presence of CsO_3 (PDF #19-0314) is established with a lesser degree of certainty in this set. The patterns of "set 2" (Figure 2b) contain the diffraction rings typical of a mixture of oxide phases and of carbonate. Whereas Cs_2O and Cs_2CO_3 (PDF #35-0962) can be assigned with a great degree of confidence, the presence of Cs_2O_2 (PDF #10-0262) and Cs_2O_3 (PDF #10-248) is less firmly established. As a rule, the characteristic 6.33 Å between the (003) planes of Cs_2O was observed only infrequently in the electron diffraction patterns, likely because of the high background intensity close to the central spot. The intensity of the (003) line in the PDF of Cs_2O is rather weak (see Figure 1), which can also explain the difficulty in observing this peak in the ED pattern. It can nevertheless be concluded that the present synthesis yields a mixture of oxide phases.

The source of the carbonate in samples 14 and 15 is not completely clear. However, these samples most likely were exposed to air at some point during their transfer from the quartz ampule to the TEM instrument. However, as far as we are aware, there was no apparent difference in the preparation or transfer of these samples compared to those of set 1. The SAED results are in reasonable agreement with the XRD and XPS measurements, even though they were carried out on different samples

CsO_2 and Cs_2O_2 have tetragonal and orthorhombic unit cells, respectively.[7,8] In both cases, the crystallographic *c* direction is parallel to the O_2 ion internuclear axis.[21] The cesium superoxide crystallizes in the calcium carbide structure with $c = 7.20$ Å and $a = 4.44$ Å, and the cesium peroxide geometry is a distorted fluorite (CaF_2) structure (O_2 replacing Ca) with $a = 4.322$ Å, $b = 7.517$ Å, and $c = 6.430$ Å. The Cs_2O has the layered "anti-$CdCl_2$" structure with a rhombohedral unit cell of dimensions 4.256×18.99 Å (18.99 is 3 times the Cs−Cs distance between adjacent layers, i.e., 3*R* symmetry). The oxygen atoms are sandwiched between two cesium layers, and Cs−Cs van der Waals interactions link adjacent "sandwiches". CsO_3 has two known phases: a monoclinic form stable at low temperatures

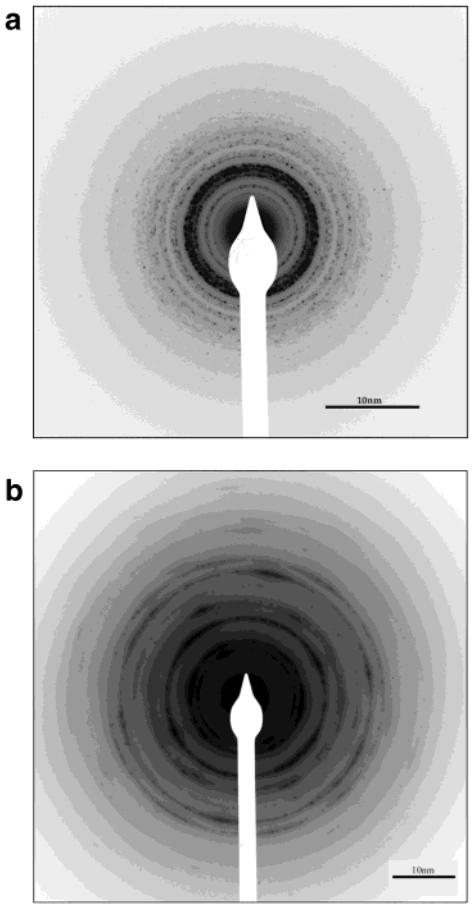

Figure 2. Selected-area electron diffraction (SAED) patterns showing the two typical sets of diffraction rings: (a) set 1, (b) set 2 (see text).

with cell dimensions of $a = 6.751$ Å, $b = 6.267$ Å, and $c = 9.015$ Å and a tetragonal form at room temperature with unit cell dimensions of $a = 9.73$ Å and $c = 8.76$ Å. The presence of the monoclinic CsO_3 in the reaction mixture has not been confirmed.

Figure 3 shows transmission electron microscopy (TEM) micrographs taken from specimens 12−15. As mentioned above, TEM observations of all of the specimens were particularly difficult to obtain because of the random movement of the crystals, as well as the bending of the crystals during observation. The random movements of the crystallites could be attributed to electron beam induced charging or dehydration (outgassing) of the crystallites. Thus, in practice, it was almost impossible to use the goniometer to tilt a crystal to the exact zone axis because of its drift and continuous change of orientation relative to the electron beam. In addition, prolonged electron irradiation led to changes of the morphology of the material: a lump with an irregular shape was formed instead of the original agglomerate consisting of individual particles (Figure 3a). The interplanar distances in Figure 3a are about 2.90−3.00 Å, and the interplanar distances in Figure 3b are about 3.45−3.55 Å. The fringes in Figure 3a correspond to interplanar distances of the (104) plane of Cs_2O (2.91 Å) or of the (130) plane of Cs_2CO_3 (2.99 Å). The fringes in Figure 3b correspond to the (012) plane of Cs_2O (3.43 Å) or the (121) plane of Cs_2CO_3 (3.45 Å).

Raman Microanalysis. Identification of the Various Phases. CsO_2, Cs_2O_2, and Cs_2O were the three main compounds identified in the synthesized mixtures. The Raman spectra reflect the crystal lattice vibrations, which are based on crystal symmetry assignments,[5,7,8] and the local vibrations of the various

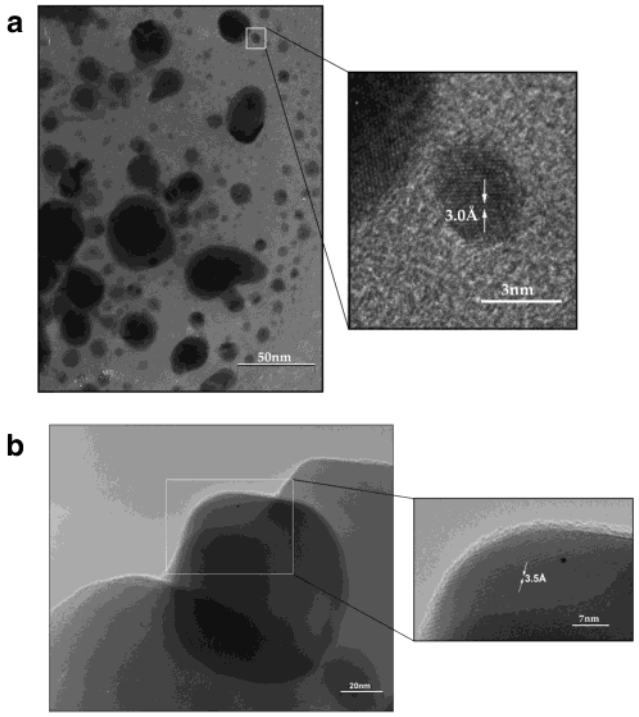

Figure 3. TEM micrographs of some typical particles in sample 15. In a, the interplanar spacing is 2.99 ± 0.04 Å; in b, the interplanar spacing is 3.55 ± 0.05 Å.

dioxide entities in the lattice (O_2^-, O_2^{2-}).[22−25] In some cases, the various cesium compounds were distributed in well-separated zones, and in other cases, mixtures of the compounds were detected on the scale of a few micrometers. The ability to distinguish between the two can be used to nondestructively monitor the quality of the cesium oxidation product.

The image shown in Figure 4a (sample 22) is constructed from two different zones that are clearly distinguished by their colors. Mapping the image with 3 μm spatial resolution indicated the presence of Cs_2O_2 in the "orange" zone exclusively, although the presence of other oxides at greater (>1 μm) depths cannot be definitively excluded. A typical spectrum of the orange zone is shown in Figure 4a. The attribution of the band at 742 cm^{-1} to the vibration of O_2^{2-} and the analysis of the peroxide ion spectrum in terms of its higher overtones and anharmonicity constant were discussed in detail elsewhere.[25] All bands other than the 742 cm^{-1} band are attributed to the Pyrex ampule. No Raman signal was obtained from the "blue" part of the sample.

Figure 4b (sample 60) presents another spectrum from a different sample. Unlike the former case, here, in addition to the peroxide ion signal at 742 cm^{-1}, a band that is attributed to O_2^- is observed at 1134 cm^{-1}. This assignment is based on the vibrational analysis of the O_2^- ion in CsO_2 that was detected at 1132 cm^{-1}.[23]

Cs_2O crystallizes in the 3*R* anti-$CdCl_2$ layered structure.[5] This structure has two interlayer Raman active modes of A_{1g} and E_g symmetries. In these optical modes, the outer sublayers of Cs^+ cations vibrate out of phase with each other while the middle sublayer of O^{2-} remains at rest. The displacement vectors are perpendicular and parallel to the basal plane in the A_{1g} and E_g modes, respectively, with the A_{1g} mode vibrating at a substantially higher frequency than the E_g mode.[26]

In Figure 4c, the Raman spectrum from one of the ampules (sample 39) is shown, revealing an anti-Stokes band at 103 cm^{-1}, attributed to the A_{1g} mode of Cs_2O.[26] Because of spectrometer characteristics, this band could not be detected in

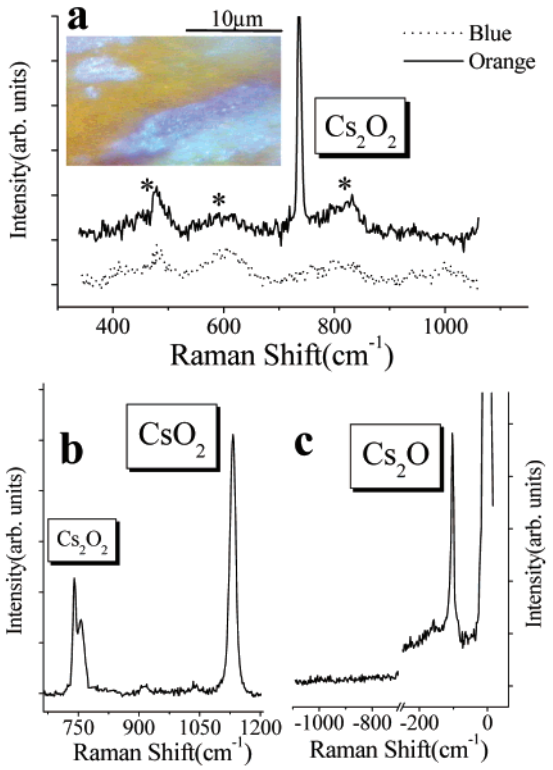

Figure 4. (a) Raman spectra from two distinct zones in sample 22 observed in the displayed image and pointed out in different colors: purple, dark appearance (dotted line); orange, bright appearance (solid line). Mapping of the image with 3-μm spatial resolution indicated the existence of Cs_2O_2 in the orange zone exclusively. All bands other than the 742 cm^{-1} band are denoted with asterisks and are attributed to the Pyrex ampule. (b) Raman spectrum (background subtracted) from sample 60 showing a mixture of CsO_2 (1134 cm^{-1}) and Cs_2O_2 (742 cm^{-1}). The origin of the band at 755 cm^{-1} is not well understood. (c) Anti-Stokes Raman spectrum from sample 39, showing a band at 103 cm^{-1} that is attributed to Cs_2O. No traces of CsO_2 and Cs_2O_2 are observed.

the Stokes side of the spectrum. The A_{1g} vibrational frequency of Cs_2O nicely correlates with a rough estimate that is acquired by comparing it to the A_1 vibration at 111 cm^{-1} of CdI_2 that crystallizes in a 4H−$CdCl_2$ structure,[26] after considering a simple linear chain dynamical model.[27] The E_g mode, which appears below 100 cm^{-1}, cannot be detected with the present instrumentation.

Monitoring of Impurities. It is important to note that no evidence for cesium carbonate was found from the Raman and XRD measurements in the samples sealed in capillaries within the glovebox. A sample of commercial Cs_2CO_3 sealed in a quartz capillary exhibited a strong Raman-active vibration at 1045 cm^{-1}. No such peak was detected in the current cesium oxide samples. The XRD patterns did not show *d* spacings corresponding to the carbonate ion either. However, TEM and XPS measurements showed traces of cesium carbonate in several samples in addition to the cesium oxides. The TEM samples were handled during transfer under argon in inflatable glovebags. It is believed that residual oxygen, water and CO_2 from the atmosphere could not be fully avoided in these glovebags. Moreover, the vapor pressure of the pumping system, which mainly consists of oil molecules, could itself be a source for carbonate formation. The XPS samples were opened in the airlock at a pressure of 0.75 bar. Here again, the residual air concentration and the oil-based pumping system were sufficient for the formation of some cesium carbonate from the extremely reactive cesium oxides. Nevertheless, the handling methods

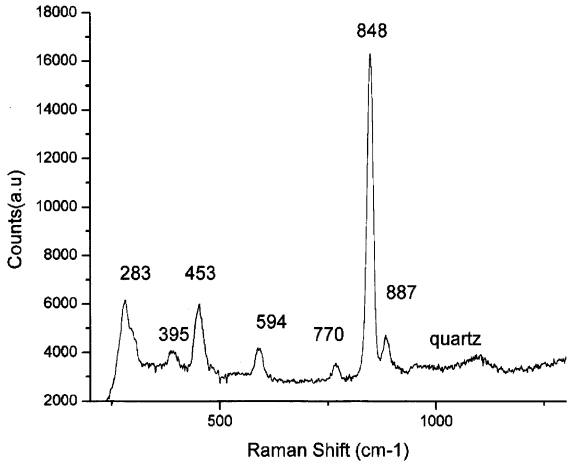

Figure 5. Raman spectrum from sample 39 showing bands that are attributed to cesium hydrate impurities.

developed during this study provided sufficient protection so that transformation of the cesium oxides to cesium carbonate was only superficial and the oxides could be discerned and analyzed.

Another possible process that might contaminate the present samples is the hydration of the oxide by residual humidity. Figure 5 presents a Raman spectrum taken from a sealed ampule (sample 39). Here, a strong band is detected at 848 cm^{-1} with weaker bands at 770 and 887 cm^{-1}, as well as some lower-frequency modes at 283, 395, 453, and 594 cm^{-1}. In accordance with Evans,[22] the band at 848 cm^{-1} is attributed to a high hydrate (possibly octahydrate) and the other bands to lower hydrates. The residual water content in the quartz ampules was shown to have a great influence on various chemical and physical processes.[28]

Optical Absorption and Luminescence. The focused excitation light sources for both absorption and luminescence measurements permitted analysis of zones with a homogeneous orange appearance (sample 9). The absorption and luminescence spectra of the orange-tinted product are presented in Figure 6a. The luminescence of the product suggests the dominance of a material with a direct band gap. The first luminescence peak, at approximately 660 nm, is due to the band-gap emission (~1.88 eV). The second emission peak, at 760 nm (1.63 eV), could be associated with a donor−acceptor relaxation of a relatively deep state. The approximate band gap of the products can be calculated from the absorption data by using the following equation[29]

$$(\alpha h\nu)^2 = h\nu - E_g$$

where α is the absorption coefficient, which is proportional to the measured optical density; $h\nu$ is the photon energy (in eV); and E_g is the calculated band gap. In Figure 6b, $h\nu$ is plotted as a function of $(\alpha h\nu)^2$. The extrapolated band gap is $E_g = 1.9$ eV, which agrees with the luminescence threshold and is consistent with previous data for Cs_2O.[15] The good fit of the experimental data suggests that the orange product is a semiconductor with a direct band gap, most probably Cs_2O or Cs_2O_2 or mixtures thereof.

Discussion

The characterization of materials that are sensitive to the ambient atmosphere is difficult. In fact, the use of multiple techniques was found to be essential for unraveling the complexity of the cesium oxide phases. Each of the above

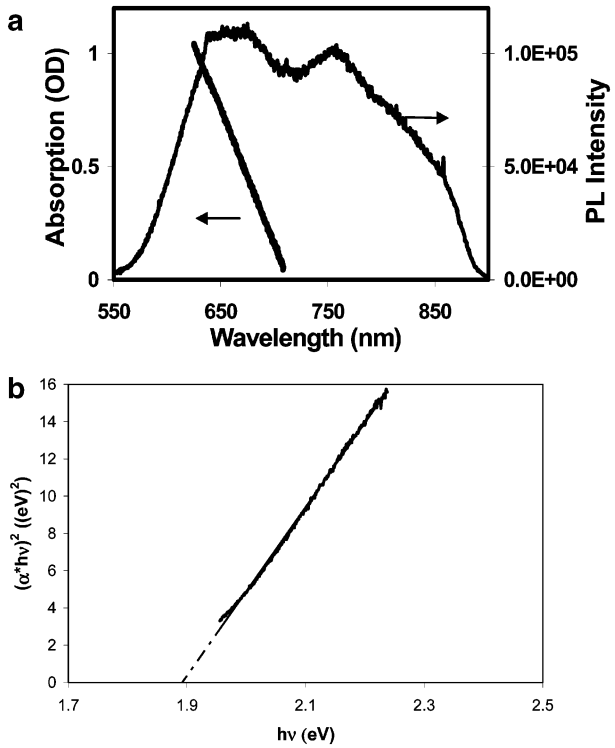

Figure 6. (a) Absorption and luminescence spectra of the cesium oxides mixture in sample 9. (b) Extrapolation of E_g from the absorption spectrum.

techniques played an important role in the analysis. The ability to make inferences from the results of one technique about the results of the other analyses was also crucial in this context. However, by all means, a most relevant tool for analysis of inhomogeneous and water-sensitive samples, such as those of the present work, was the TEM/EDS/ED. This kind of analysis had not been used before for the analysis of the oxides of cesium. Raman microscopy was also essential in establishing the contamination of the samples by carbonate during manipulation or handling. It was also useful for the analysis of hydrates, which were formed by reaction of the cesium oxides with residues of water adsorbed to the ampule walls. The XPS results clearly showed the progressive surface oxidation.

Careful homogenization of the reactants, a lengthy thermal annealing process, and the gradual heating/cooling of the ampule were used to attain chemical equilibrium. Furthermore, numerous experiments (not reported in this work) were carried out during which a number of experimental parameters were varied in a systematic way. These experiments did not provide a clear relationship between the experimental conditions and the reaction products. The calculated free energies, at room temperature, of the formation of both the peroxide (Cs_2O_2) and the superoxide (CsO_2) are very high (−327 and −387 kJ/mol, respectively), whereas that of Cs_2O is somewhat lower (−274 kJ/mol).[30] Therefore, Cs_2O can disproportionate into a mixture of peroxides and elemental cesium, which could further react with oxygen to give the superoxides. The relatively modest difference between the free energies of formation of the cesium peroxide and superoxide might explain the difficulty in obtaining a pure reaction product. However, the predominance of CsO_2 in the analyzed samples was expected because of its greater thermodynamic stability. Also, the very high free energy of formation of Cs_2CO_3 (−1019 kJ/mol) might explain the high chemical reactivity of the cesium oxides with respect to ambient CO_2, although the free energies of the reactions of CO_2 with the various oxides are not as negative as that of the reaction of the respective elements.

Conclusions

The present study shows a comprehensive analysis of the air-sensitive products of the reaction between cesium and oxygen. Both direct lattice imaging and electron diffraction modes of TEM indicate that a mixture of oxides was obtained in this reaction. The diffraction lines of the XRD patterns can be associated with more than one oxide, again demonstrating the heterogeneous character of the present product. Chemical analysis by EDS in TEM showed the variation of the Cs/O ratios from different locations on the grids. These ratios are consistent with the oxide, peroxide, and superoxide of cesium. The chemical shifts of the oxygen XPS lines clearly attest to the presence of the oxide, peroxide, and superoxide ions, as well. Surface oxidation of the samples indicates that an improved handling of the samples would be needed for future studies. The chemical analysis also establishes the absence of impurities in most of the ampules, although the presence of residual water in the ampule wall is problematic. Optical measurements (absorption and luminescence) show that, in accordance with previous works, direct band-gap semiconductors with $E_g \approx 1.9$ eV were obtained for the orange-tinted phase, which could be ascribed to Cs_2O or Cs_2O_2. Raman spectroscopy provided evidence for the unique spectral vibrations of the peroxide and superoxide oxygen ions, giving further support to the previous findings. Furthermore, these measurements established that the products of the synthesis were cesium oxides with no traces of cesium carbonate. Cesium carbonate was obtained only during improper handling of the samples during transfer prior to analysis. Also, the Raman bands at 103, 742, and 1134 cm^{-1} were assigned to the oxide, peroxide, and superoxide ions of cesium, respectively.

A methodology of this kind could be very useful in the study of cesium oxide coatings in photoemissive devices as a means for their characterization, particularly with respect to their aging mechanisms.

Acknowledgment. This work was supported by a grant in aid from the Minerva Foundation (Munich) and the G.M.J. Schmidt Minerva Center for Supramolecular Architecture.

References and Notes

(1) Howe, J. L. *J. Am. Chem. Soc.* **1907**, *29*, 384.
(2) Marquis, R. *Bull. Soc. Chem.* **1907**, *1*, 169.
(3) Rengade, E. *Ann. Chim. Phys. VIII* **1907**, *11*, 379.
(4) Rengade, E. *Ann. Chim. Phys. VIII* **1907**, *11*, 381.
(5) Tsai, K. R. *J. Phys. Chem.* **1956**, *60*, 338.
(6) Tsai, K. R. *J. Phys. Chem.* **1956**, *60*, 347.
(7) Foppl, H. *Z. Anorg. Allg. Chem.* **1957**, *291*, 12.
(8) Dudarev, V. Ya.; Tsentsiper, A. B.; Dobrolyubova, M. S. *Sov. Phys. Crystallogr.* **1974**, *18*, 477.
(9) Helms, A.; Klemm, W. *Z. Anorg. Allg. Chem.* **1939**, *242*, 201.
(10) Sommer, A. H. *J. Appl. Phys.* **1980**, *51*, 1254.
(11) Su, C. Y.; Lindau, I.; Spicer, W. E. *Chem. Phys. Lett.* **1982**, *87*, 523.
(12) Woratschek, B.; Sesselmann, W.; Kuppers, J.; Ertl, G.; Haberland, H. *J. Chem. Phys.* **1987**, *86*, 4.
(13) Jupille, J.; Dolle, P.; Besancon, M. *Surf. Sci.* **1992**, *260*, 271.
(14) Krawietz, T. R.; Murray, D. K.; Haw, J. F. *J. Phys. Chem. A* **1998**, *102*, 8779.
(15) Borzyak, P. G.; Bibik, V. F.; Kramerenko, G. S. *Bull. Acad. Sci. USSR, Phys. Ser.* **1956**, *20*, 939.
(16) Phillips, C. C.; Hughes, A. E.; Sibbett, W. *J. Phys. D: Appl. Phys.* **1984**, *17*, 611.
(17) Ramqvist, L.; Hamrin, K.; Johansson, G.; Fahlman, A.; Nordling, C. *J. Phys. Chem. Solids* **1969**, *30*, 1835.

(18) Hammond, J. S.; Gaarenstroom, S. W.; Winograd, N. *Anal. Chem.* **1975**, *47*, 2194.
(19) Gammond, J. S.; Holubka, J. W.; Devries, J. E.; Duckie, R. A. *Corros. Sci.* **1981**, *21*, 239.
(20) Buller, R.; Cohen, H.; Popovitz-Biro, R.; Minkin, E.; Lifshitz, E.; Lahav, M. *Adv. Funct. Mater.* **2002**, *12*, 713.
(21) Pedio, M.; Benfatto, M.; Aminpirooz, S.; Hasse, J. *Phys. Rev. B* **1994**, *50*, 6596.
(22) Evans, J. C. *Chem. Commun.* **1969**, 682.
(23) Hunter-Saphir, S. A.; Creighton, J. A. *J. Raman Spectrosc.* **1998**, *29*, 417.
(24) Eysel, H. H.; Thym, S. *Z. Anorg. Allg. Chem.* **1975**, *411*, 97.
(25) Livneh, T.; Band, A.; Tenne, R. *J. Raman Spectrosc.* **2002**, *33*, 675.
(26) Adams, D. M.; Tan, T. *J. Phys. Chem. Solids* **1981**, *42*, 559.
(27) Anderson, A.; Lo, Y. W.; Todoeschuck, J. P. *Spectrosc. Lett.* **1981**, *14*, 301.
(28) Schäfer, H.; Grofe, T.; Trenkel, M. *J. Solid State Chem.* **1973**, *8*, 14.
(29) Pankove, J. I. *Optical Processes in Semiconductors*; Dover Publications Inc.: New York, 1971; p 36.
(30) Bard, A. J.; Parsons, R.; Jordan, J. *Standard Potentials in Aqueous Solution*; Marcel Dekker Inc.: New York, 1985; pp 755−757.